photonics

MDPI

Article

Synchronous Mark Design Based on Collinear Holographic Data Storage System to Improve Reconstruction Efficiency

Ruying Xiong, Lin Peng, Xu Zheng, Junhui Wu, Hongjie Liu * and Xiaodi Tan *

Key Laboratory of Opto-Electronic Science and Technology for Medicine of Ministry of Education, Fujian Provincial Key Laboratory of Photonics Technology, College of Photonic and Electronic Engineering, Fujian Normal University, Fuzhou 350117, China; qsz20231402@student.fjnu.edu.cn (R.X.); qsx20230809@student.fjnu.edu.cn (L.P.); qsz20231362@student.fjnu.cn (X.Z.); qbx20230105@yjs.fjnu.edu.cn (J.W.)

* Correspondence: qbx20220092@yjs.fjnu.edu.cn (H.L.); xtan@fjnu.edu.cn (X.T.)

Abstract

A collinear holographic data storage system stores two-dimensional information in the three-dimensional spatial domain of the medium, offering features such as high speed, high density, and long lifespan, making it a promising technology for the future of data storage. However, a collinear holographic data storage system is limited by the alignment error of the optical system and is also sensitive to environmental noise and external interference, which increases the reading error. When recording and reading holographic storage materials, synchronous marks are used for positioning to correct data misalignment. Therefore, optimizing synchronous mark design of data pages is crucial for improving storage stability and reading accuracy. In this paper, we propose a star-shaped synchronous mark to replace the square-shaped synchronous mark, which improves the holographic grating coupling efficiency. Experimental results show that this method enhances reconstruction strength and reduces reading errors caused by external factors. The star-shaped synchronous mark achieves a better spectral match with the reference pattern, yielding a stronger diffracted signal. Experimental results show that this method reduces the bit error rate by approximately 25% compared to square-shaped synchronous marks under displacement multiplexing.

Keywords: holographic storage; synchronous mark; data page

1. Introduction

With the rapid development of information technology, the amount of new data globally is growing exponentially, and traditional data storage technology can no longer meet the demand [1,2]. The next-generation data storage technology urgently requires a breakthrough. Holographic data storage technology has become an ideal choice for the new generation of data storage due to its advantages, such as large capacity, high transmission rate, and long storage life [3–8]. It adopts page-oriented technology, records two-dimensional data pages in three-dimensional storage media, and combines multiplexing technology to achieve efficient storage [9–12]. Among various multiplexing techniques, shift multiplexing draws inspiration from the mechanism of disk drives [13,14]. It enables data storage by altering the relative position between the reference beam and the object beam, while also mitigating the influence of medium thickness on Bragg selectivity. As a result, it represents a readily implementable method for increasing storage density.

The traditional off-axis holographic storage system uses separate reference and object beams, offering high diffraction efficiency but with a complex optical path and sensitivity

Check for updates

Received: 19 March 2026
Revised: 27 April 2026
Accepted: 28 April 2026
Published: 29 April 2026

to vibrations [15,16]. Computer-generated holography technology eliminates the need for a reference optical path and can use incoherent light sources, making the system more compact and vibration-resistant [17,18]. However, computer-generated holography technology still faces challenges such as high computational complexity, which restricts its application in high-density data storage. In contrast, the collinear holographic data storage system adopts a coaxial optical path, completing both recording and readout through a single objective lens, offering advantages in optical simplicity and system stability, and enabling simple data decoding. A typical collinear system employs a digital micromirror device (DMD) to load an information pattern consisting of a data page and a reference pattern, and the interference between the signal beam and the reference beam forms a holographic grating within the photosensitive medium.

In practical applications, the amplitude holographic data storage system using a DMD can achieve a data page switching speed of 20 kHz, demonstrating significant advantages [19,20]. The system performs high-precision data page encoding in units of pixels to maximize the capacity of a single data page [21–24]. However, such high-precision encoding also brings challenges: even a one-pixel displacement during data retrieval can cause many errors. Therefore, amplitude holographic data storage systems mostly rely on synchronous marks for data retrieval [25]. After capturing the reconstructed data page with a camera, the synchronous marks can accurately locate the data page to achieve highly accurate data reading.

However, after long-term storage or displacement multiplexing of traditional data pages, the error rate significantly increases even if the data part remains intact. This is because square-shaped synchronous marks consist of large contiguous blocks of white pixels, which contain predominantly low spatial frequencies. In contrast, the reference pattern has a radially distributed ring-shaped structure with mid-to-high spatial frequencies. This spectral mismatch reduces Bragg matching between the reference beam and the square mark, causing the diffracted signal of the square-shaped synchronous mark to drop below the detection threshold more rapidly than that of the data pixels under shift multiplexing or material shrinkage. As a result, the square-shaped synchronous marks attenuate faster than the data parts, leading to inaccurate positioning and thus increasing the data error rate [26].

To address this issue, this paper proposes a new star-shaped synchronous mark, which has a higher coupling efficiency with the radiation-shaped reference light during data recording. Compared with the traditional synchronous mark, the diffraction efficiency is significantly improved, providing a strong guarantee for precise data positioning.

In this paper, we propose a star-shaped synchronous mark to replace the square-shaped synchronous mark in the collinear holographic data page, to avoid the reconstruction intensity of the synchronous mark being lower than that of the data, thereby increasing the possibility of dislocation of reconstruction data. Our approach regards the cosine similarity on the Fourier plane of the image as the spectral similarity, and the pattern of the synchronous mark is determined through the spectral similarity analysis between the reference pattern and the synchronous mark [27]. On this basis, we conducted aging and displacement multiplexing experiments on the collinear holographic data storage system. The results indicate that the star-shaped synchronous marks enhance reconstruction intensity and avoid the impact of factors such as optical system aberration, medium deformation, and environmental changes on positioning.

2. Experimental Setup and Methods

All experiments in this study are conducted based on the collinear holographic data storage system, whose optical path configuration is shown in Figure 1.

https://doi.org/10.3390/photonics13050438

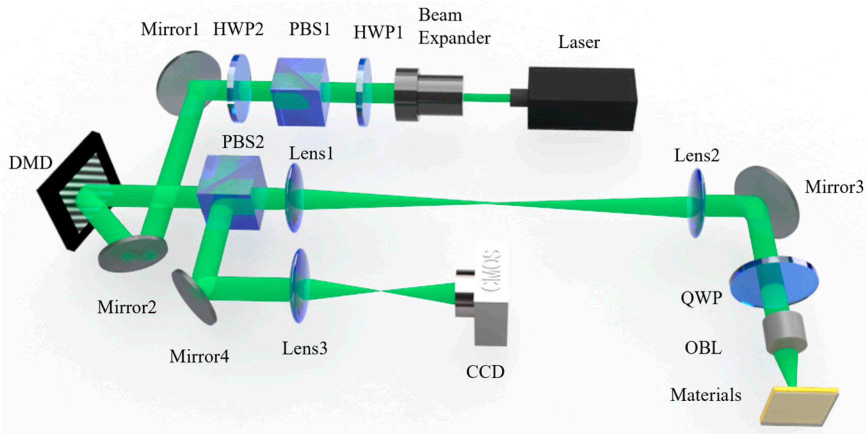

Figure 1. Experimental optical path of the collinear holographic data storage system. HWP: half-wave plate; PBS: polarization beam splitter; QWP: quarter-wave plate; DMD: digital micromirror devices; DBS: dichroic beam splitter; CCD: charge-coupled device; OBL: objective lens. PBS1 is used for both beam splitting and polarization selection. The splitting ratio is adjusted by the half-wave plate to control the light intensity incident on the DMD. HWP1 and PBS1 are used together to adjust the light intensity incident on the DMD, and HWP2 is used to adjust the polarization direction for efficient beam transmission.

The green laser beam, whose wavelength is 532 nm, first passes through a beam expander and then is projected onto the DMD via a mirror. During recording, a composite beam consisting of the data page and reference pattern is loaded onto the DMD. The information light and reference light are then focused onto the holographic material by a 4f system and an objective lens. The two beams interfere with each other to form a hologram, which is recorded. During reading, the reference pattern is loaded onto the DMD, and the diffracted information light is reflected into the optical path by a reflective material. Since the information light passes through the QWP twice, it is reflected by the PBS onto a CCD, where the reconstructed information pattern is captured. The holographic storage material we used is phenanthrenequinone-doped polymethyl methacrylate photopolymer (PQ/PMMA) [28].

The following experimental parameters were used in this work: a 532 nm laser, an exposure time of 2s per hologram, a PQ/PMMA material thickness of 0.5 mm, a total of 40 holograms in the shift multiplexing experiment, an aging temperature of 80 °C, and an aging duration of 240 h.

Within the information pattern of the collinear holographic storage system, synchronous marks serve as critical elements for achieving precise data localization and decoding.

The illustration of the information pattern in the collinear holographic data storage system is shown in Figure 2. The information pattern comprises two primary components: the data page and the reference pattern. The system employs an amplitude-modulated data page format that consists of 51 sub-pages and a data page synchronous mark. The data page synchronous mark is positioned at the top-left corner of the data page, while 51 sub-page synchronous marks are positioned in the center of the sub-page. A common synchronous mark is a solid dot block with a 4×4 pixel arrangement, referred to as a square-shaped synchronous mark.

In the recording process, the data page and reference uploaded to the spatial light modulator converge with the holographic material on the Fourier plane, interfering with each other to form a recording stripe. Due to the difference between the square-shaped synchronous mark spatial frequency and reference pattern frequency, even a slight deviation from the Bragg condition can lead to a rapid decline in the coupling efficiency of the holographic grating. Consequently, the reconstructed synchronous marks exhibit low intensity, which hinders data readout and causes decoding difficulties even when the information pixels remain intact. This is because, in collinear holographic storage systems, the decoding of reconstructed data pages primarily relies on the precise identification and registration of synchronous marks. This decoding process consists of three key steps: First, the matrix corresponding to the synchronous mark structure used during recording is employed as a convolution kernel to perform cross-correlation with the reconstructed image. By detecting the response peaks, the coordinate positions of the reference synchronous marks are preliminarily determined. Second, the convolution operation is repeated in the neighborhood of these reference points to locate adjacent synchronization marks. By calculating the ratio of the pixel distance between them to the theoretical design value, the geometric scaling factor and overall shift in the reproduced image are derived, thereby establishing an accurate coordinate mapping relationship. Finally, based on these geometric parameters, individual data subpage regions are extracted and compared pixel by pixel with the original encoded data to compute system performance metrics such as the bit error rate and signal-to-noise ratio. It is worth noting that if the convolution response peaks are not prominent due to noise interference or optical distortion in the reproduced image, synchronous mark identification may fail. In such cases, registration errors propagate to subsequent data processing steps, causing the calculated bit error rate to contain significant systematic registration deviations.

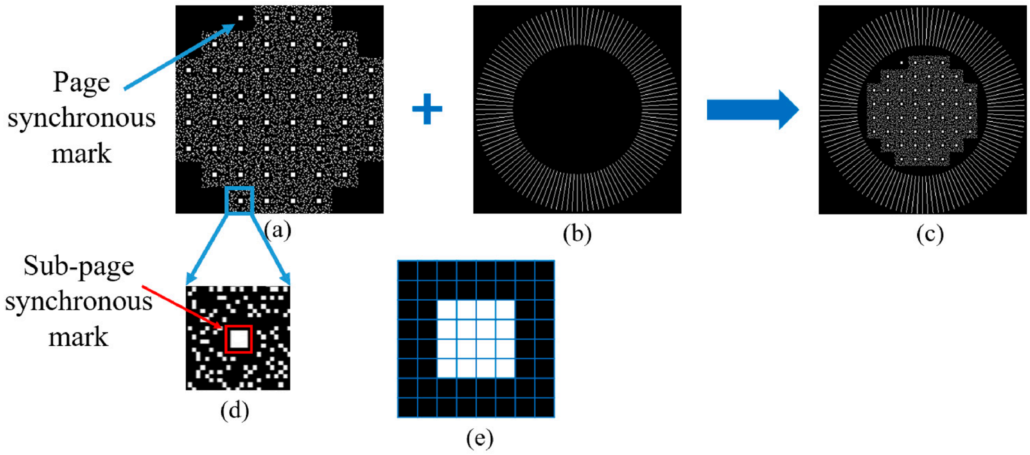

Figure 2. (**a**) Data page; (**b**) reference pattern; (**c**) information pattern; (**d**) sub-page; (**e**) square-shaped mark.

Under low diffraction efficiency, synchronous marks may fall below the detection threshold and vanish before data pixels when their signal-to-noise ratio deteriorates, causing data page localization failure and effective data loss despite intact data integrity. As shown in Figure 3, failed synchronous mark identification under low reconstruction intensity can result in a bit error rate as high as 80%. This indicates that conventional synchronous marks are not directly applicable to collinear holographic storage systems, necessitating redesign of their structural configuration and physical characteristics. This phenomenon becomes particularly pronounced under high storage density and multiple write-read cycles, leading to increased localization errors and degraded decoding accuracy.

To address this, this study focuses on optimizing the energy distribution of the convolution kernel, constructing several synchronous mark patterns with similar total numbers of bright pixels (ranging from 13 to 16) but varying shapes, as schematically illustrated in Figure 4.

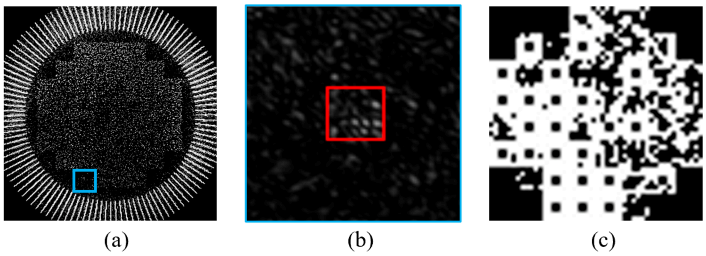

Figure 3. Impact of difficult-to-recognize synchronous marks on decoding performance. (**a**) Reconstructed data page image under low diffraction intensity; (**b**) enlarged view of the synchronous marks in the data page (the blue box in (**a**) indicates the enlarged region); (**c**) bit error rate distribution map (white pixels indicate errors).

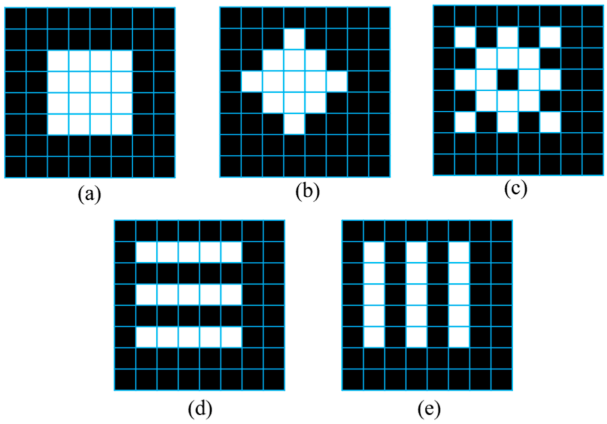

Figure 4. Schematic diagram of different-shaped synchronous mark patterns. (**a**) Traditional square-shaped synchronous mark; (**b**) diamond-shaped synchronous mark; (**c**) star-shaped synchronous mark; (**d**) horizontal line synchronous mark; (**e**) vertical line synchronous mark.

To quantitatively evaluate the simulation effect of synchronous marks, this paper defines the matching degree based on the Fourier plane spectrum similarity. According to Fourier optics theory, the spatial frequency distribution of volume holographic gratings determines their Bragg selectivity characteristics. By mapping the spatial distributions of the reference and synchronous marks to the frequency domain, the overlap degree of their dominant spatial frequency components can be directly reflected, thereby indirectly indicating the Bragg matching condition [29]. Let the complex amplitude distribution of the reference beam at the reconstruction plane be $r(x, y)$ and the spatial distribution corresponding to the synchronous mark structure be $l(x, y)$. Their two-dimensional Fourier transforms are given in Equations (1) and (2), respectively.

$$R(u, v) = \mathcal{F}\{r(x, y)\} \tag{1}$$

$$L(u, v) = \mathcal{F}\{l(x, y)\} \tag{2}$$

where (u, v) are the spatial frequency coordinates at the Fourier plane, and $\mathcal{F}\{\cdot\}$ denotes the two-dimensional Fourier transform. To eliminate the influence of light intensity variations and quantify the spectral overlap degree, as shown in Equation (3), the matching degree M is defined as the normalized inner product:

$$M = \frac{\sum_{u,v} | R(u, v) | | L(u, v) |}{\sqrt{\sum_{u,v} | R(u, v) |^2} \sqrt{\sum_{u,v} | L(u, v) |^2}} \tag{3}$$

https://doi.org/10.3390/photonics13050438

This metric satisfies $M \in [0,\ 1]$, where a larger value indicates a higher spectral overlap between the reference beam and the synchronous mark, corresponding to better Bragg matching. When the matching degree is high, the diffraction signal of the synchronous mark during reconstruction is concentrated and stable. Conversely, when the matching degree is low, Bragg mismatch intensifies, making the localization performance more sensitive to displacement perturbations and noise.

Cosine similarity measures the similarity between two images by evaluating the directional agreement of their feature vectors in a high-dimensional space [30]. The core concept involves representing each image's high-level features as vectors and computing the cosine of the angle between them to quantify their resemblance. This method is insensitive to the magnitude of the feature vectors, focusing instead on the relative distribution patterns of the features. As a result, it effectively mitigates disturbances caused by variations in illumination and scale. Therefore, it is well-suited for evaluating the spectral similarity between the synchronous marks and the reference pattern in this study. The formula for cosine similarity is shown in Equation (4):

$$\text{cosine\_similarity}(A, B) = \frac{A \cdot B}{\| A \| \| B \|} = \frac{\sum_{i=1}^{n} A_i B_i}{\sqrt{\sum_{i=1}^{n} A_i^2} \sqrt{\sum_{i=1}^{n} B_i^2}} \quad (4)$$

The cosine similarity value ranges from [−1, 1], where −1 indicates complete dissimilarity, and 1 indicates complete similarity. Here, A and B are the flattened vectors of two images. The matching degree M is used for theoretical analysis of the spectral overlap between the reference beam and the synchronous mark on the Fourier plane, while cosine similarity serves as a practical metric for comparing candidate patterns and selecting the optimal one. Both metrics quantify the similarity between spectral distributions. In this work, cosine similarity is adopted for quantitative comparison and final pattern selection.

Figures 5 and 6 illustrate the spectrograms of the synchronous mark and the reference pattern, respectively. Cosine similarity is computed on the flattened magnitude spectrograms.

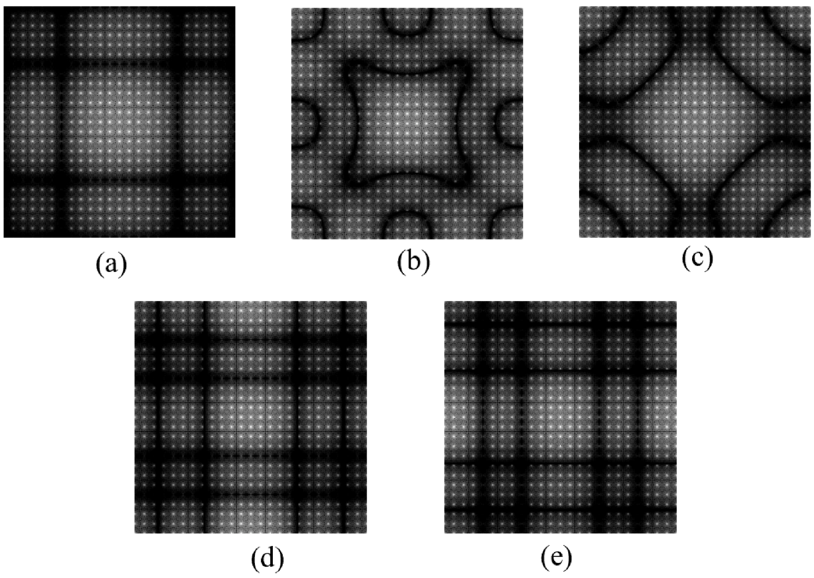

Figure 5. Spectrum surface pattern of different-shaped synchronous mark patterns. (**a**) Traditional square-shaped synchronous mark; (**b**) diamond-shaped synchronous mark; (**c**) star-shaped synchronous mark; (**d**) horizontal line synchronous mark; (**e**) vertical line synchronous mark.

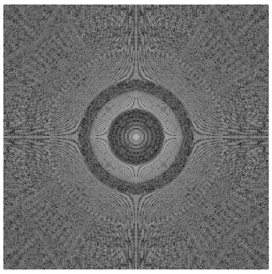

Figure 6. Spectrum surface pattern of the reference pattern.

The corresponding cosine similarity between each synchronous mark and the reference pattern was subsequently computed, and the experimental results are listed in Table 1. The experimental results show that the star-shaped synchronous mark achieves the highest cosine similarity with the reference pattern; therefore, it was selected for subsequent experiments.

Table 1. Cosine similarity.

Square-Shaped	Diamond-Shaped	Star-Shaped	Horizontal Line	Vertical Line
0.7831	0.8121	0.8305	0.7457	0.7615

3. Experiments and Results

Based on this, we designed a series of experiments, such as the displacement multiplexing experiment and aging experiment. We calculate their bit error rate and brightness percentage to evaluate the performance of the star-shaped synchronous mark. The brightness percentage is defined as the ratio of the sum of pixel intensities within the target region to the sum of the maximum possible pixel intensities in that region.

In the collinear holographic storage system, we recorded information patterns with two kinds of synchronous marks under the same recording conditions, as shown in Figure 7. The bit error rate (BER) of the square-shaped synchronous mark in the reconstructed image was approximately 1%, while the BER of the star-shaped synchronous mark was below 0.5%.

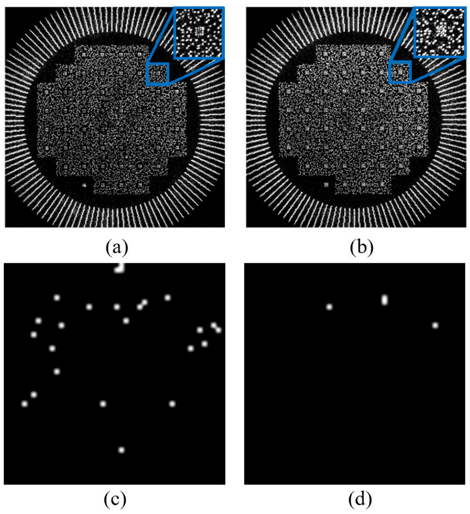

Figure 7. Traditional and modified information patterns with corresponding local enlarged views. (**a**) The square-shaped synchronous mark information pattern. (**b**) The star-shaped synchronous mark information pattern. (**c**) The square-shaped synchronous mark information reconstruction error distribution. (**d**) The star-shaped synchronous mark information reconstruction error distribution.

Each information pattern consisted of 51 synchronous marks. We calculated the brightness percentage of all synchronous marks in the reconstructed images, as shown in Figure 8. Due to external factors such as the non-uniformity of the recording material and system vibrations, differences in brightness percentages among the synchronous marks were observed. In the reconstructed images, the brightness percentage of all star-shaped synchronous marks is higher than that of square-shaped ones.

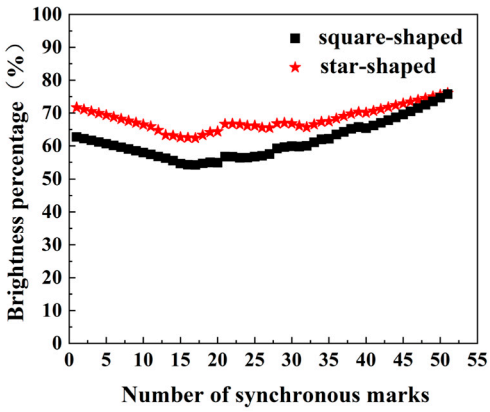

Figure 8. The brightness percentage of different synchronous marks in reconstruction images.

Shift multiplexing is a key method for achieving high-density volume holographic data storage. This technique enables the recording of a new hologram at the Bragg-mismatched position of the previous one, ensuring that multiple holograms can be reconstructed without crosstalk, thereby enabling multiplexed storage and significantly increasing storage density. The 10 μm shift interval is determined based on the theoretical Bragg selectivity of the system to minimize crosstalk between adjacent holograms. However, the photosensitive medium for holographic materials is limited, and the shift-multiplexing spacing between holograms is small, resulting in each holographic grating having weak intensity, which in turn leads to reduced diffraction intensity. We designed an experiment with alternating multiplexing of 40 square-shaped synchronous mark and star-shaped synchronous mark information patterns at 10 μm intervals to verify whether the star-shaped synchronous mark can achieve accurate information decoding under high-density recording.

In the alternating multiplexing experiment, because the recording and reconstruction effects of each image were uneven, we conducted the square-star-shaped and star-square-shaped experiments in sequence. The experimental results are shown in Figures 9 and 10. The difference between Figures 9 and 10 lies in the order of alternating multiplexing. Figure 9 shows the case where square-shaped marks were recorded first, followed by star-shaped marks. Figure 10 shows the opposite order. This design was intended to exclude the influence of recording order on the experimental results. In the displacement multiplexing experiment, the average bit error rate for the square-shaped synchronous mark is 3.87%, while that for the star-shaped synchronous mark is 3.14%, an absolute reduction of approximately 0.63%. The bit error rate for the square-shaped synchronous mark fluctuates between 1% and 5% across the 40 alternating multiplexed recordings, while that for the star-shaped synchronous mark ranges from 0.5% to 4%. It should be noted that both marks exhibit certain fluctuations, which may be attributed to inhomogeneities in the photosensitive material and minor mechanical vibrations of the system during the prolonged multiplexing process. Nevertheless, the star-shaped synchronous mark consistently achieves lower bit error rates than the square-shaped synchronous mark at all measurement points, demonstrating better stability.

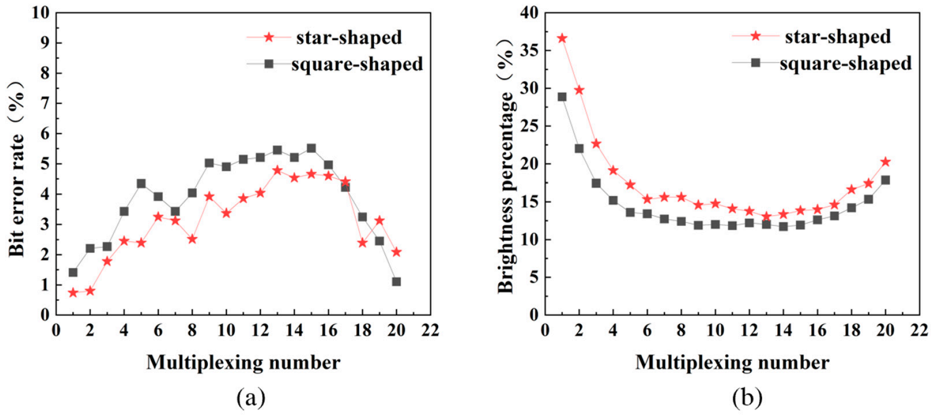

Figure 9. Alternating multiplexing of square-shaped synchronous mark and star-shaped synchronous mark information patterns. (**a**) Bit error rate. (**b**) Brightness percentage.

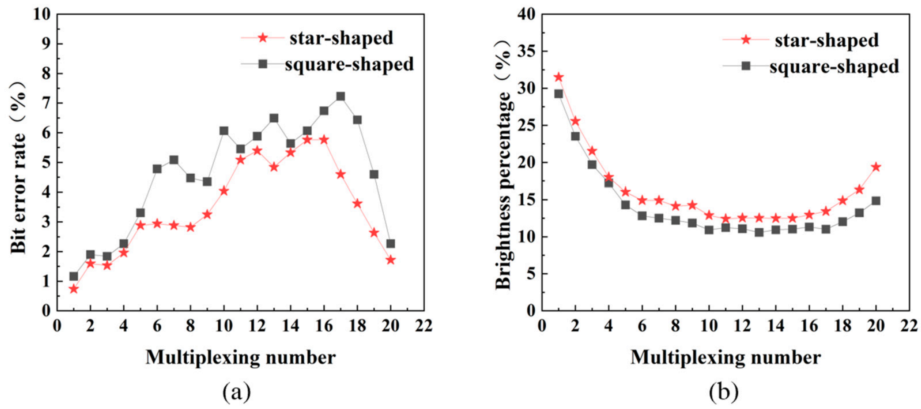

Figure 10. Alternating multiplexing of star-shaped synchronous mark and square-shaped synchronous mark information patterns. (**a**) Bit error rate. (**b**) Brightness percentage.

Besides storage density, storage lifetime is also a critical performance metric in holographic data storage. We subjected the holographic material recorded with square-shaped synchronous mark and star-shaped synchronous mark information patterns to an accelerated aging test in a harsh environment (80 °C) to simulate its storage lifetime. The aging temperature of 80 °C is selected because it approaches the glass transition temperature of the PQ/PMMA photopolymer, which accelerates the aging process without causing structural damage to the material. As shown in Figure 11, the experimental results indicate that the longer the material is stored, the more significantly the new information pattern outperforms the old one in terms of bit error rate.

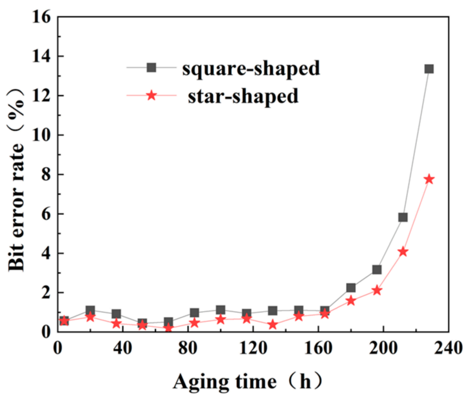

Figure 11. The brightness percentage of different synchronous marks in reconstructed images.

4. Conclusions

This paper proposes a star-shaped synchronous mark design to replace traditional marks. Experimental results demonstrate that the star-shaped synchronous mark exhibits higher Fourier spectrum similarity with the reference pattern, leading to a holographic grating with improved coupling efficiency and consequently stronger reconstructed signal intensity. Calculations of cosine similarity confirm this spectral alignment, which enhances the robustness of the synchronous symbol under material inhomogeneity and environmental variations. This high degree of spectral similarity stems from the geometric correspondence between the synchronous mark and the reference beam profile used during recording. The star-shaped structure, with its radially distributed features, effectively approximates the spatial frequency components of the reference pattern, thereby enabling more efficient energy transfer during the reconstruction process. This underlying principle suggests that the design methodology is not limited to a specific shape; rather, it can be extended to other reference beam profiles by maximizing spectral similarity. Compared to conventional marks, the new design maintains superior optical performance even under degraded grating conditions, significantly improving decoding accuracy and reducing bit error rate. These findings suggest that the star-shaped synchronous mark can enhance the reliability and performance of holographic storage systems, providing a valuable and extensible strategy for future development in high-density data storage.

Author Contributions: Conceptualization, R.X. and H.L.; methodology, R.X. and L.P.; validation, R.X. and X.Z.; writing—original draft preparation, R.X. and J.W.; writing—review and editing, R.X. and X.T.; supervision, X.T. All authors have read and agreed to the published version of the manuscript.

Funding: This research was funded by the National Natural Science Foundation of China, under the grant number U22A2080.

Data Availability Statement: The data underlying the results presented in this paper are not publicly available at this time but may be obtained from the authors upon reasonable request.

Conflicts of Interest: The authors declare no conflicts of interest.

References

1. Horimai, H.; Tan, X. Holographic information storage system: Today and future. *IEEE Trans. Magn.* **2007**, *43*, 943–947. [CrossRef]
2. Lin, X.; Hao, J.; Zheng, M.; Dai, T.; Li, H.; Ren, Y. Optical holographic data storage-the time for new development. *Opto-Electron. Eng.* **2019**, *46*, 180642. [CrossRef]
3. Hao, J.; Lin, X.; Lin, Y.; Chen, M.; Chen, R.; Situ, G.; Horimai, H.; Tan, X. Lensless complex amplitude demodulation based on deep learning in holographic data storage. *Opto-Electron. Adv.* **2023**, *6*, 220157. [CrossRef]
4. Lin, Y.; Ke, S.; Song, H.; Liu, H.; Yang, R.; Lin, D.; Li, X.; Zheng, J.; Cao, Q.; Hao, J.; et al. Anti-noise performance analysis in amplitude-modulated collinear holographic data storage using deep learning. *Opt. Express* **2024**, *32*, 29666–29677. [CrossRef]
5. Márquez, A.; Li, C.; Beléndez, A.; Maier, S.; Ren, H. Information multiplexing from optical holography to multi-channel metaholography. *Nanophotonics* **2023**, *12*, 4415–4440. [CrossRef]
6. Li, J.; Hu, P. Highly sensitive photopolymer for holographic data storage. *Opt. Express* **2022**, *30*, 40599–40610. [CrossRef]
7. Hegner, M. The light fantastic. *Nature* **2002**, *419*, 125–127. [CrossRef]
8. Gao, H.; Fan, X.; Xiong, W.; Hong, M. Recent advances in optical dynamic meta-holography. *Opto-Electron. Adv.* **2021**, *4*, 210030. [CrossRef]
9. Nobukawa, T.; Nomura, T. Multilevel recording of complex amplitude data pages in a holographic data storage system using digital holography. *Opt. Express* **2016**, *24*, 21001–21011. [CrossRef] [PubMed]
10. Leith, E.; Kozma, A.; Upatnieks, J.; Marks, J.; Massey, M. Holographic Data Storage in Three-Dimensional Media. *Appl. Opt.* **1966**, *5*, 1303–1311. [CrossRef]
11. Ayres, M.; Hoskins, A.; Curtis, K. Image oversampling for page-oriented optical data storage. *Appl. Opt.* **2006**, *45*, 2459–2464. [CrossRef]
12. Li, H.; Zhao, C.; Li, J.; Xu, H.; Xu, W.; Tan, Q.; Song, C.; Shen, Y.; Yao, J. Spin-dependent amplitude and phase modulation with multifold interferences via single-layer diatomic all-silicon metasurfaces. *Opto-Electron. Sci.* **2025**, *4*, 240025. [CrossRef]

13. Li, K.; Wang, Y.; Pi, D.; Li, B.; Luan, H.; Fang, X.; Chen, P.; Lu, Y.; Gu, M. Multi-dimensional multiplexing optical secret sharing framework with cascaded liquid crystal holograms. *Opto-Electron. Adv.* **2024**, *7*, 230121. [CrossRef]
14. Zheng, S.; Tan, J.; Liu, H.; Lin, X.; Saita, Y.; Nomura, T.; Tan, X. Orthogonal matrix of polarization combinations: Concept and application to multichannel holographic recording. *Opto-Electron. Adv.* **2024**, *7*, 230180. [CrossRef]
15. Tatsuro, I. Formularization and simulation of Bragg selectivity of readout signals in angular-multiplexing holographic data storage. *Appl. Opt.* **2016**, *55*, 2664–2674. [CrossRef] [PubMed]
16. Nobuhiro, K.; Tetsuhiko, M.; Norihiko, I.; Koji, K.; Hiroshi, K.; Naoki, S.; Osamu, M. Half-data-page insertion method for increasing recording density in angular multiplexing holographic memory. *Appl. Opt.* **2011**, *50*, 2361–2369. [CrossRef]
17. Naru, Y.; Yusuke, S.; Takanori, N. Binary computer-generated-hologram-based holographic data storage. *Appl. Opt.* **2019**, *58*, 3083–3090. [CrossRef]
18. Saita, Y.; Matsumoto, A.; Yoneda, N.; Takanori, N. Multiplexed recording based on the reference wave correlation for computer-generated holographic data storage. *Opt. Rev.* **2020**, *27*, 391–398. [CrossRef]
19. Xu, J.; Lin, Y.; Zhong, L.; Ke, Y.; He, C.; Lin, S.; Lin, D.; Lin, X.; Tan, X. Matching for realizing high-speed reading in holographic data storage system. *Opt. Express* **2024**, *32*, 46259. [CrossRef]
20. Dudley, W.; Duncan, M.; Slaughter, J. Emerging digital micromirror device (DMD) applications. *Proc. SPIE* **2003**, *4985*, 14–25. [CrossRef]
21. King, B.; Neifeld, M. Sparse modulation coding for increased capacity in volume holographic storage. *Appl. Opt.* **2000**, *39*, 6681–6688. [CrossRef]
22. Horimai, H.; Tan, X.; Li, J. Collinear holography. *Appl. Opt.* **2005**, *44*, 2575–2579. [CrossRef]
23. Burr, G.; Ashley, J.; Coufal, H.; Grygier, R.; Hoffnagle, J.; Jefferson, C.; Marcus, B. Modulation coding for pixel-matched holographic data storage. *Opt. Lett.* **1997**, *22*, 639–641. [CrossRef]
24. Wu, Y.; Yang, Q.; Shen, B.; Tao, Y.; Zhang, X.; Tao, Z.; Xing, L.; Ge, Z.; Li, T.; Bai, B.; et al. Multifunctional mixed analog/digital signal processor based on integrated photonics. *Opto-Electron. Sci.* **2024**, *3*, 240012. [CrossRef]
25. Liu, J.; Horimai, H.; Lin, X.; Liu, J.; Huang, Y.; Tan, X. Optimal micro-mirror tilt angle and sync mark design for digital micro-mirror device based collinear holographic data storage system. *Appl. Opt.* **2017**, *56*, 4779–4784. [CrossRef]
26. Meng, Y.; Lu, Y.; Zhang, P.; Liu, Y.; Yin, F.; Kai, L.; Yang, Q.; Chen, F. High-frequency enhanced ultrafast compressed active photography. *Opto-Electron. Adv.* **2025**, *8*, 240180. [CrossRef]
27. Zhang, Z.; Li, G.; Liu, Y.; Wang, H.; Hoenders, B.J.; Liang, C.; Cai, Y.; Zeng, J. Robust measurement of orbital angular momentum of a partially coherent vortex beam under amplitude and phase perturbations. *Opto-Electron. Sci.* **2024**, *3*, 240001. [CrossRef]
28. Hu, P.; Chen, Y.; Li, J.; Wang, J.; Liu, J.; Wu, T.; Tan, X. Impact of fullerene on the holographic properties of PQ/PMMA photopolymer. *Compos. Sci. Technol.* **2022**, *221*, 109335. [CrossRef]
29. Yu, Y.W.; Teng, T.C.; Hsieh, S.C.; Cheng, C.Y.; Sun, C.C. Shifting selectivity of collinear volume holographic storage. *Opt. Commun.* **2010**, *283*, 3895–3900. [CrossRef]
30. Chanwimalueang, T.; Mandic, D. Cosine similarity entropy: Self-correlation-based complexity analysis of dynamical systems. *Entropy* **2017**, *19*, 652. [CrossRef]